Polymer 51 (2010) 2383–2389

Contents lists available at ScienceDirect

Polymer

journal homepage: www.elsevier.com/locate/polymer

Orientation analysis of individual electrospun PE nanofibers by transmission electron microscopy

Taiyo Yoshioka [a,*], Roland Dersch [b], Masaki Tsuji [c], Andreas K. Schaper [a,*]

[a] Material Sciences Center, Philipps University of Marburg, 35032 Marburg, Germany
[b] Department of Chemistry, Philipps University of Marburg, 35032 Marburg, Germany
[c] Institute for Chemical Research, Kyoto University, Uji, Kyoto-fu 611-0011, Japan

ARTICLE INFO

Article history:
Received 10 December 2009
Received in revised form
14 March 2010
Accepted 19 March 2010
Available online 27 March 2010

Keywords:
Electrospinning
Molecular orientation
Shish-kebab structure

ABSTRACT

A systematic orientation analysis of individual electrospun polyethylene (PE) nanofibers was performed by transmission electron microscopy (TEM). PE nanofibers with a wide diameter distribution, ranging from 150 nm to several micrometers, and a variety of morphologies, including cylindrical, beaded- and ribbon-like fibers, were produced by the high-temperature solution electrospinning. In each fiber, crystalline orientation and its morphology were investigated by TEM. In the cylindrical fibers, development of fiber structure was strongly related to the fiber diameter. Depending on the diameter, three different structural models based on 1) the random-oriented crystalline structure, 2) the shish-kebab structure, and 3) the fibrillar structure composed of extended-chain crystals were proposed. In addition, orientation analysis of beaded fibers and that of ribbon-like fibers was also performed.

1. Introduction

Electrospinning is a versatile technique to fabricate polymeric nanofibers; it has been attracting much attention in basic research as well as in various fields of nanofiber applications as sensors, catalyst supports, or in tissue engineering [1–3]. The technique, which is based on the elongational action of an electrostatic force-field, is often envisaged to be easily performed according to its rather simple setup; however, the electrospinning process actually involves many physical instabilities which are far from being understood [4–8]. Well known phenomena resulting from those instabilities are random jet passes, a broad distribution of the fiber diameter, and non-uniformity of the fiber morphology. As to the thinning of the fiber during the electrospinning process, Reneker and his group have reported a number of interesting experimental observations as well as theoretical considerations [4,5,9]. They experimentally clarified that non-continuous thinning occurs by perturbation of the jet path due to bending instabilities. Once the perturbation happens, the straight jet path changes into a three-dimensional coiled path, and this allows the jet to become elongated much more than a straight jet path. The perturbation usually repeats several times, and every occurrence of a new perturbation reduces the diameter of the coil path as well as of the fiber itself. Besides this primary thinning process Reneker et al. observed a second process which is based on the branching of an originally thick fiber into many thin fibers [4,5,9]. It is reasonable to assume that in both processes the thinner fibers are subjected to stronger bending instabilities, and experience a longer jet path, which is synonymous with a more intense action of elongational force.

In most reports on electrospinning experiments, the diameter and the morphology of the resulting fiber products have been carefully analyzed and controlled. Furthermore, several approaches have been worked out to describe the jet pass theoretically [4–8]. On the contrary, the fine structure of the fibers, the degree of orientation of the molecular chains, of the crystallites, and of the ordered superstructures, have not been analyzed to the same degree. In many cases, only average data on the fiber structures obtained by, for example, X-ray diffraction (XRD), infrared spectroscopy (IR), and differential scanning calorimetry (DSC), was discussed. Although attempts have been made to study the non-averaged structure of single nanofibers using atomic force microscopy (AFM) [10], Raman spectroscopy [11], and transmission electron microscopy (TEM) [12,13], the influence of the diameter and morphology on the fiber structure has not been clarified in these studies. A more detailed understanding of the microprocesses of the fiber formation and structure is needed for improving the mechanical, electrical, and optoelectronic properties, and for tailoring the compatibility to living cells as scaffolds in tissue engineering.

* Corresponding authors. Tel.: +49 6421 282 3456; fax: +49 6421 282 3383.
E-mail addresses: yoshioka@staff.uni-marburg.de (T. Yoshioka), dersch@staff.uni-marburg.de (R. Dersch), tsujimas@scl.kyoto-u.ac.jp (M. Tsuji), schaper@staff.uni-marburg.de (A.K. Schaper).

0032-3861/$ – see front matter © 2010 Elsevier Ltd. All rights reserved.
doi:10.1016/j.polymer.2010.03.031

The present paper deals with the electrospinning behaviour of polyethylene (PE), which, due to its simple backbone structure, serves as a model polymer in research on orientation-induced crystallization processes [14]. Only a few reports have appeared on the electrospinning of PE to date, because of serious experimental difficulties due to the lack of an appropriate solvent at room temperature and because of the poor electrical conductivity of PE. Practical answers to attain successful electrospinning of PE will be found by spinning from the melt [15] or from high-temperature solution [15–18]. Givens et al. [16] prepared PE fibers from *p*-xylene solution including a small amount of salt at 105–110 °C, which had quite a large diameter in the micrometer range and very rough surface morphology. They collected their fibers using a conventional flat collector. The fibers showed an orthorhombic crystalline structure with about 55% crystallinity measured by Raman spectroscopy and XRD, but the crystal orientation was not determined. On the other hand, Rein et al. [17] electrospun PE fibers with a minimum diameter of 200 nm from a mixture of *p*-xylene and cyclohexanone at 120 °C and collected them using a rotating collector at 300 m/min. XRD of bundles of parallel aligned nanofibers revealed oriented as well as non-oriented crystals. Thus, both works [16,17] provide average crystalline information from multifiber bundles and therefore it is not possible from these studies to distinguish between the actual structure of an individual fiber and the superposition of structures of different kinds of fibers in the bundle.

We have adopted the high-temperature solution electrospinning of PE, because on that route it should be possible to fabricate fibers much thinner fibers with a more developed fiber structure than in melt electrospinning. While recent studies have demonstrated that the molecular orientation of electrospun fibers can be strongly influenced by particular methods of collection, e.g. using either a parallel-electrode collector [19] or a rotating disc collector [20], this study focuses on the fine structure, especially on the molecular orientation, of the as-spun PE fibers and ribbons independently of the collecting system. For that purpose a conventional flat collector was applied, which allows the analysis of the basic orientation processes and avoids any post-spinning structural modifications. Structural studies were carried out by transmission electron diffraction (TED) and TEM of individual nanofibers.

2. Experimental

2.1. Materials

High-density PE pellets (Hostalen GD 6250; weight average molecular weight: $M_w = 100{,}000$, and average density: 0.95 g/cm^3), *p*-xylene (Sigma–Aldrich, Inc.) and tetrabutylammonium hydrogen sulfate (t-BAHS) (Sigma–Aldrich, Inc.) were used as the starting materials. The PE pellets and the t-BAHS salt, which serves to enhance the electrical conductivity of the solution, were dissolved in *p*-xylene at 115 °C with mild stirring for 3 h. The appropriate PE concentration was determined in preliminary experiments to be 3 wt%, and the t-BAHS concentration to be 0.2 wt%. It should be emphasized that we have also successfully performed the electrospinning of PE from solution without the inclusion of salt. These experiments confirmed that mixing this amount of the salt makes the spinning process more stable without, however, affecting the observations reported in this manuscript.

2.2. Electrospinning

In order to perform high-temperature electrospinning experiments of PE solutions, an infrared (IR) heating system (500 W, 220 V) (Mor Electric Heating Assoc., Inc., USA) was combined with the conventional electrospinning setup (Fig. 1). The glass syringe with a metallic spinneret was set in the center of a pair of the two ceramic IR emitters of dimension 60 × 120 mm, so that the whole syringe including the tip of the spinneret was exposed directly by IR radiation. The temperature variation, detected directly at the lateral side of the syringe, was within ±0.5 °C during a spinning cycle of several minutes.

The starting solution was transferred into the glass syringe, which was preheated to 112 °C. Electrospinning was performed at different applied voltages from 10 to 30 kV, and at various spinning distances of 100–350 mm between the tip of the spinneret and the collector. The fibers were collected on small pieces of silicon wafers for examination by SEM and on copper grids covered with thin carbon film for TEM investigations, both placed on the aluminum foil collector.

2.3. Characterization

Morphological observations of the fibers were carried out in a field emission scanning electron microscope JSM-7500F (JEOL Ltd., Japan) at an accelerating voltage of 4 kV, after platinum coating of the fibers. Crystallographic analysis of single nanofibers was done by selected-area electron diffraction (SAED) in a transmission electron microscope JEM-3010 (JEOL Ltd., Japan) at an accelerating voltage of 300 kV using a slow scan CCD camera (Gatan Inc., USA) for recording images and SAED patterns. In order to suppress electron charge-up and to support each fragile fiber on the grid, copper grids covered with thin carbon film were used. Thin aluminum coating of the specimens was applied for calibrating the diffraction camera length.

3. Results and discussion

A typical low-magnification SEM image of PE fibers prepared by electrospinning at 25 kV with a spinning distance of 300 mm is

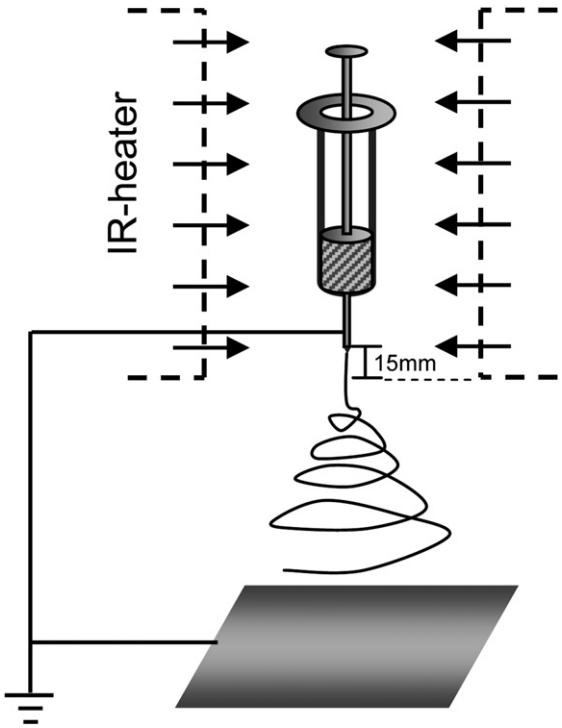

Fig. 1. Experimental setup of the high-temperature electrospinning with IR-heating system.

shown in Fig. 2(a). A spinning distance longer than 200 mm was preferable for successful fiber collection without re-dissolving, otherwise a number of fibers re-dissolved and adhered to the collector. The collected fibers showed a broad diameter distribution from 150 nm to several micrometers and also various types of surface morphologies from very smooth to very rough. As a general rule, the fibers of thinner diameter show a smooth surface morphology (Fig. 2(b)), and the fibers with diameters >2 μm a very rough surface (Fig. 2(c)) similar to the one reported by Givens et al. [16]. In addition to the usual cylindrically shaped fibers, a certain amount of beaded fibers (see Section 3.2) and ribbon-like fibers (see Section 3.3) have been found. The lateral dimensions of the beads range from several hundred nanometers to several tens of micrometers, the width of the ribbons ranges from several hundreds nanometers to tens of micrometers.

3.1. Orientation analysis of cylindrical PE fibers

3.1.1. Analysis of the morphology and the molecular orientation

Fig. 3(a)–(d) and (a′)–(d′) show bright-field TEM images of single fibers of different diameter and their corresponding SAED patterns. All SAED patterns show sharp crystalline reflections of orthorhombic PE crystals; however, the crystal orientation varies remarkably when one goes from the 1.38 μm thick fiber (Fig. 3(a)) to the 620 nm (Fig. 3(b)), and the 350 nm fibers (Fig. 3(c) and (d)). In Fig. 4 the fiber diameter is plotted against the central angle (α) (see Fig. 3(b″)) for the 110 and 200 equatorial arc-shaped reflections in the SAED patterns, obtained from 30 fibers including the fibers shown in Fig. 3. Here, the central angle for the equatorial arc-shaped reflections corresponds to the angular orientation distribution of the 110 and 200 lattice planes and the smaller α means the higher uniaxial-fiber orientation of the crystals (or crystallites). This plot shows a tendency that the thinner diameter fibers possess the higher degree of orientation, and the crystal orientations can be classified into roughly three different groups related to the angular orientation distribution of the crystals: i) random orientation ($\alpha = 180°$); ii) low orientation with an angular width ranging from 60 to 120°; and iii) high orientation with the angular range of less than 60°. This classification corresponds to three different diameter ranges: i) thicker than 1 μm; ii) 400 nm–1 μm; and iii) thinner than 400 nm. Within class iii), two different levels of orientation based on the appearance of the 002 meridional reflection and additional high-order reflections occur. As shown in the SAED pattern (Fig. 3(d′)), and its model image (Fig. 3(d″)), the quite highly ordered orientation pattern was also observed in the orientation class iii), and is distinguished in Fig. 4 from the orientation level of Fig. 3(c″). These observations indicate that the XRD result reported by Rein et al. [17] was a superposition of different orientation levels of the cylindrical fibers depending on the fiber diameter.

The diffraction patterns presented above of the fibers in the orientation classes ii) and iii) are in agreement with a stacked-lamellar [21] to shish-kebab structure [22,23]. In practice, the clear stacked-lamellar structure is sometimes revealed by close inspection of the electrospun PE fibers using SEM (Figs. 5 and 6) and TEM (Fig. 7(a)), and the structure can also be seen in the TEM bright-field images in Fig. 3(b) and (c) (the structure in these two figures is not clearly resolved, however one can see the structure especially the edge of the fibers). These morphological observations and the orientation analysis prove that the fibers in the orientation classes ii) and iii) have the stacked-lamellar structure or shish-kebab structure. The SEM image (Fig. 5) clearly reveals the fiber being composed of a bundle of shish-kebab-like entities with diameters of about 150 nm each. The several shish-kebabs are in a densely packed almost hexagonal order. Almost all of the lamellae within the shish-kebabs have a curved shape which disturbs the perfection of the lamellar stacking along the fiber axis. Wang et al. [24] explained the lamellar curving by merging of the lamellae due to capillary forces with increasing size. These curved lamellae cause the arc-shaped equatorial reflections in the diffraction patterns of classes ii) and iii). Fig. 6 showing two fibers with different diameters of 280 and 580 nm supports this hypothesis well. The position of the assumed shish entity is represented by a broken line while several kebabs are traced by solid lines (see Fig. 6(b) and (c)). The comparison of Fig. 6(b) and (c)) shows that the diameter of each shish-kebab-like entity, as well as the degree of curvature of the lamellae, are larger in the thicker fiber than in the thinner one. Thus, it is considered that these differences in orientation level in the classes ii) and iii) are closely related to the variation of the deviation angle (θ) (see Fig. 3(b‴)) of stacked lamellae from the direction perpendicular to the fiber axis. On the other hand, the morphological image in Fig. 3(d) shows several smooth fibril-like entities (indicated with arrows in the inset) instead of the shish-kebab structure. The image contrast of these fibril-like entities is considered to be based on the diffraction contrast due to a highly ordered crystalline phase. It can be concluded therefore that this crystalline phase is formed by well-aligned almost extended-chain molecules.

The hierarchical structural components in the single electrospun fiber are more likely to be distinguished in fibers that experienced some stretching deformation. Fig. 7 presents a comparison of a non-fibrillated portion of a single fiber (Fig. 7(a)–(c)) and a highly fibrillated portion (Fig. 7(d)–(g)). The fibrillation occurred occasionally when the TEM grid was removed from the aluminum foil collector. A similar fibrillar deformation after solidification, induced by the mechanical stretching due to the rotating disc collector, in electrospun fibers of poly(ethylene oxide) was observed by Zussman et al. [25]. The original fiber in Fig. 7(a) with a diameter of 450 nm shows, at first glance, a stacked-lamellar structure with a large curvature of each lamella. On the other hand, the fibrillated portion shows that the original fiber was stretched

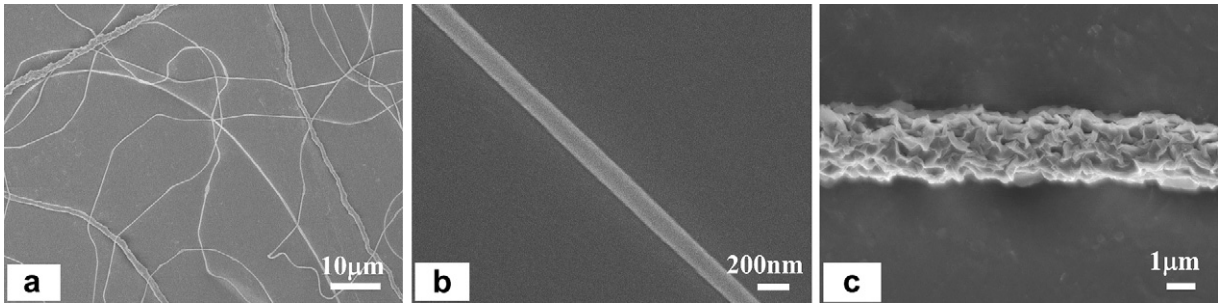

Fig. 2. (a) Typical SEM image of PE fibers electrospun at 25 kV at a spinning distance of 300 mm. The SEM images (b) and (c) show the typical smooth and rough surface morphologies of thin and thick fibers, respectively.

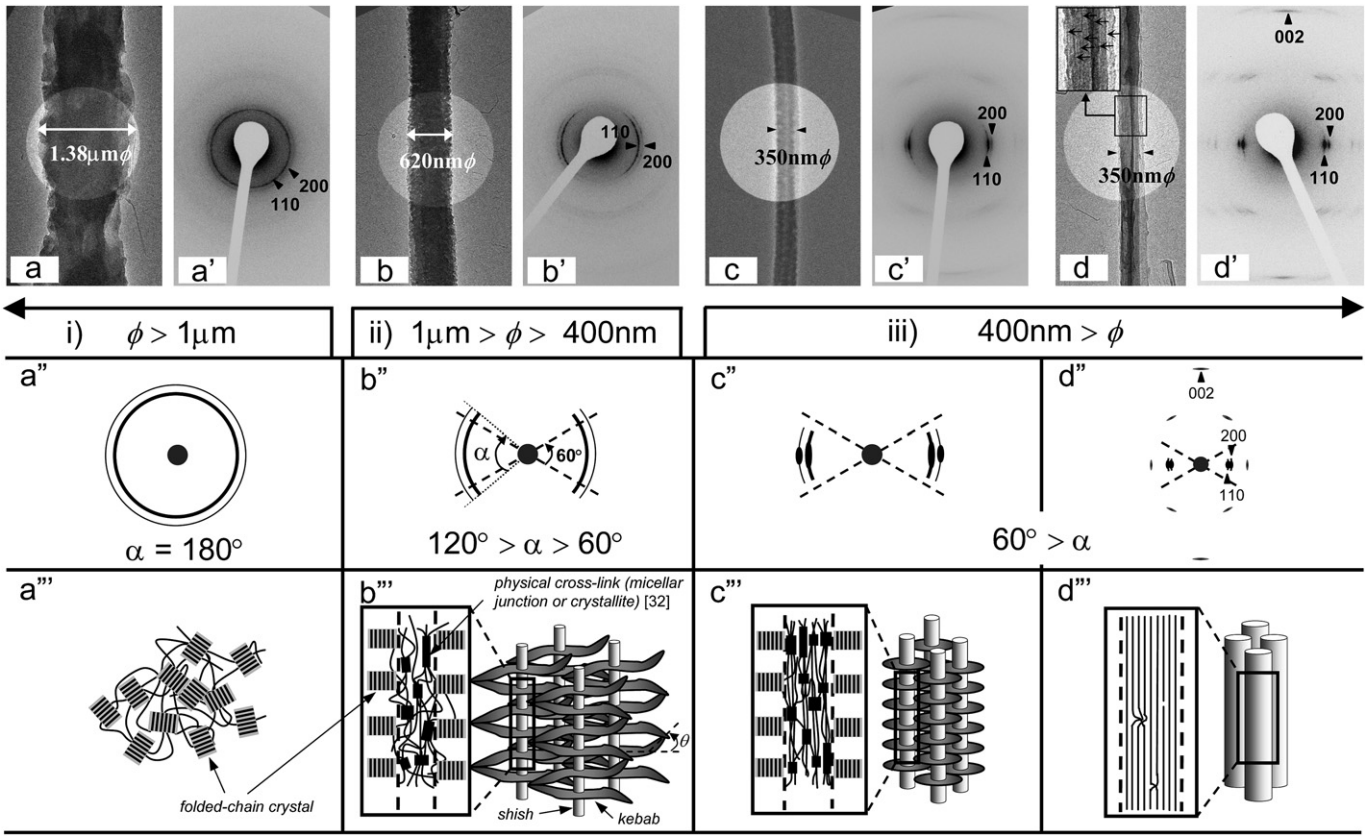

Fig. 3. Bright-field TEM images of electrospun PE fibers of different diameters (a–d), corresponding SAED patterns obtained from each single fiber (a′–d′), schematic reflection patterns (a″–d″), and models of fiber structures for each fiber diameter (a‴–d‴). The angles of (α) and (θ) in b″ and b‴ represent "the central angle" for the 110 and 200 equatorial arc reflections in the SAED pattern and "the deviation angle" of curved stacked lamellae from the direction perpendicular to the fiber axis, respectively.

and separated in places with a connection through a lot of fine fibrils. It is well known that in the stacked-lamellar structure, adjacent lamellar crystals are connected through a great number of tie-chains [26,27], and if the structure is stretched along the fiber axis, each lamellar crystal becomes unfolded through the action of tie-chains forming a number of almost extended-chain fibrils [26,28–32]. Based on previous knowledge, such fibrils are each independent of each other as shown at A and B in Fig. 7(e). Besides these independent fibrils, a somewhat thicker fibrillar entity is detected (see C in Fig. 7(e)), guided with the arrows directed downwards in Fig. 7(d), which continuously runs through the core of the fiber over some micrometer distance thereby crossing several kebab lamellae. It is suggested that this long fibrillar entity, which is revealed by its strong diffraction contrast, represents the original

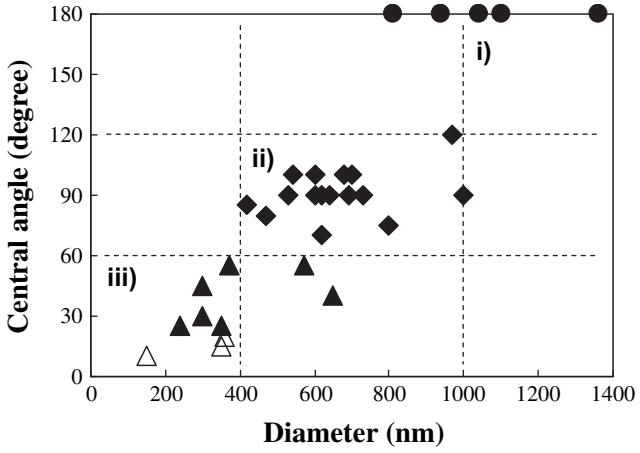

Fig. 4. Relationship between the central angle (α; see Fig. 3) for the 110 and 200 equatorial arc-shaped reflections in the SAED patterns and the fiber diameter. The filled circle indicates random orientation ($\alpha = 180°$), the filled diamond low orientation ($60° < \alpha < 120°$), and the filled triangle high orientation ($60° > \alpha$). The open triangle indicates quite high ordered orientation patterns with the appearance of the 002 meridional reflection and additional high-order reflections.

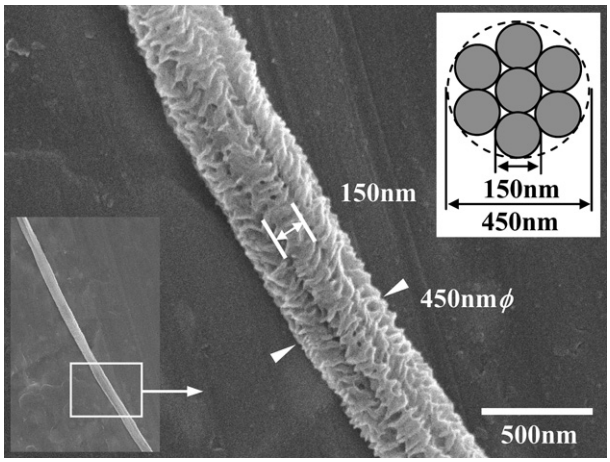

Fig. 5. SEM image of an electrospun PE fiber showing the shish-kebab-like entities. The lower left inset shows a low-magnification overview, the upper right inset a schematic image of a fiber axis projection of seven shish-kebabs (encircled in grey) in an almost close-packed hexagonal order. The spinning condition was 25 kV with a spinning distance of 300 mm.

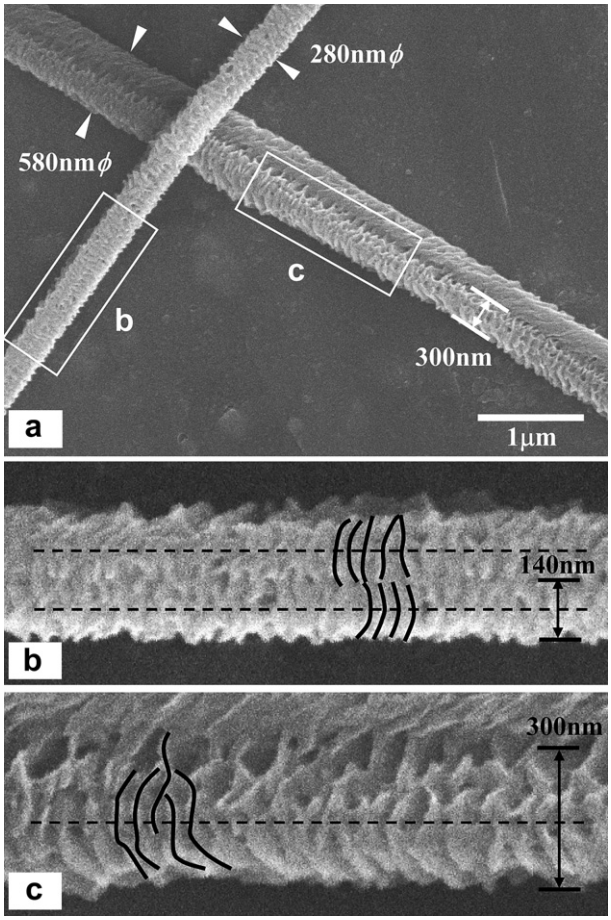

Fig. 6. SEM image of electrospun PE fibers showing shish-kebab-like morphology (a). The magnified images (b) and (c) are from the rectangular areas of the thinner and thicker fibers, respectively. The broken lines in (b) and (c) represent the center lines of each shish-kebab, the curved solid lines in (b) and (c) trace several representative kebabs. The spinning condition was 25 kV with a spinning distance of 300 mm.

backbone shish somewhat stretched during the tensional deformation. Another shish structure is observed at D in Fig. 7(e), guided with the arrows directed upwards in Fig. 7(d). The SAED pattern Fig. 7(g) taken from the fibrillated part demonstrates that both types of fibrils are composed of almost extended-chain crystals. From these observations it can be concluded that during electrospinning the first formed long fibrils act as backbones for the lamellar overgrowth perpendicular to the fiber axis.

3.1.2. Formation mechanism of the fiber structure

In our experimental setup, the surrounding environment of the spun fibers was not heated except for the first 15 mm below the tip of the spinneret (see Fig. 1). Even if detection of the environmental temperature close to the IR-heater is very difficult, at a point 30 mm below the spinneret temperatures lower than 50 °C could be measured. Thus, after escaping the spinneret, the hot spinning-solution jet would quickly cool down to near the crystallization temperature for PE of ~90 °C [33] within a distance of less than 30 mm. During this step, i.e. before significant thinning occurs, an unoriented gel structure is formed in which micellar junctions and small folded-chain nuclei act as physical cross-links [33,34]. In the successive spinning process, the gel structure changes into different orientational states depending on the elongational forces and the multiple branching of the jet due to instabilities. The resulting fibers of the thinnest diameter class iii) are subjected to the strongest elongational force for the longest

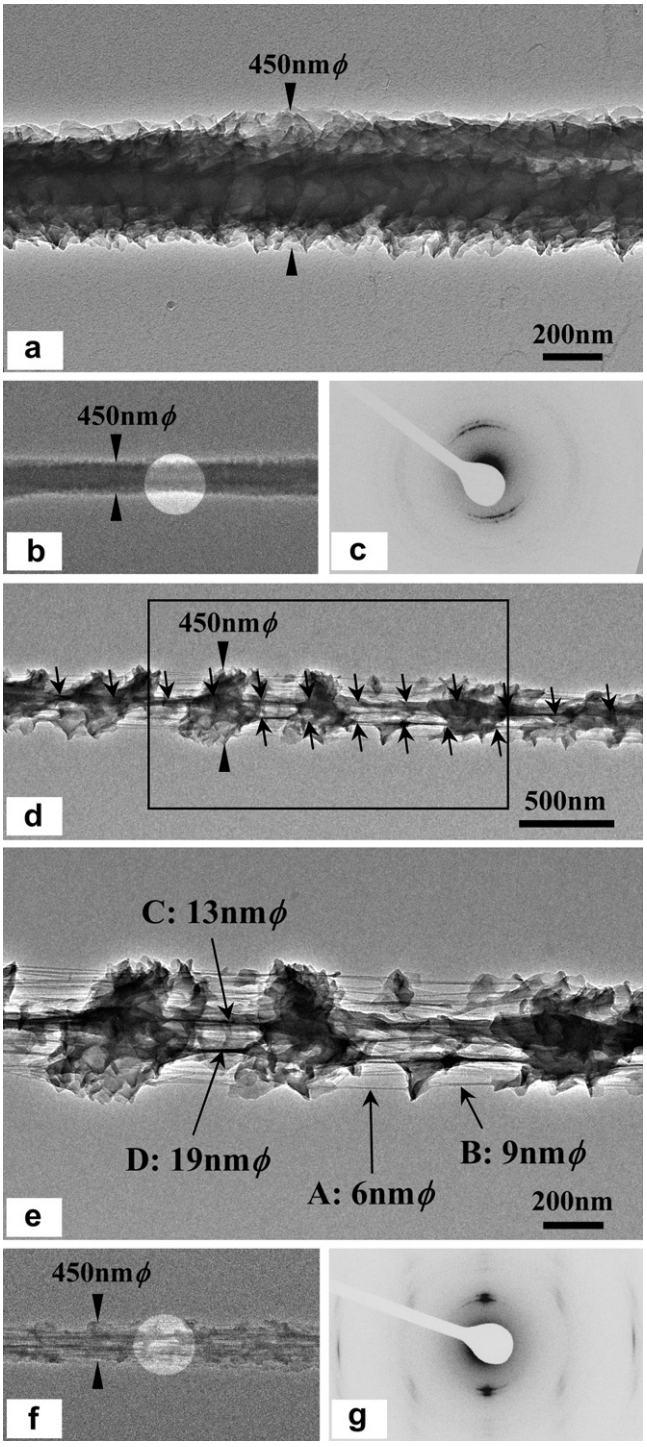

Fig. 7. TEM analysis for a partly fibrillated single fiber. Bright-field image (a), its defocus contrast image (b) including the image of the SAED aperture and the corresponding SAED pattern (c) are from a non-fibrillated portion. The bright-field image (d), the enlarged image (e) of the rectangular area in (d), its defocus contrast image (f) including the image of the SAED aperture and the corresponding SAED pattern (g) are from fibrillated portions. The spinning condition was 25 kV with a spinning distance of 300 mm.

time leading to the formation of a highly fibrous state of fully elongated molecular chains (Fig. 3(d″)). The remaining crystallizable free chains of the gel network successively crystallize epitaxially [23,35] or "soft epitaxially" [36,37] on the fibrous entities at a later stage (Fig. 3 (c‴)).

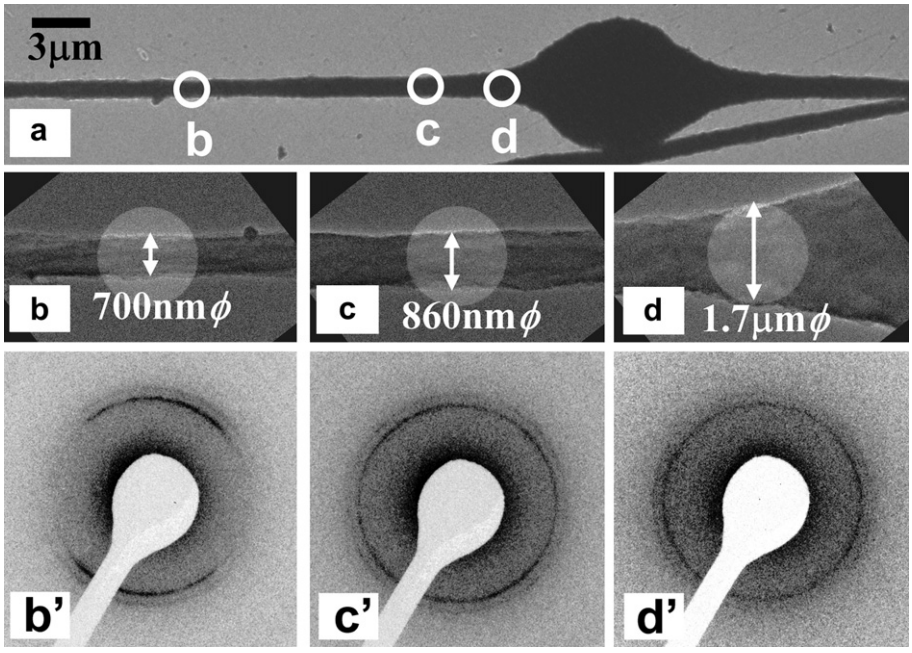

Fig. 8. Sequence SAED analysis for a single beaded fiber. The SAED pattern (b′) was obtained from the straight part (b) far from the bead, the pattern (c′) from the almost straight part (c) but near the bead, and the pattern (d′) from the end of the bead. The spinning condition was 25 kV with a spinning distance of 300 mm.

In the fibers categorized in class ii), the diameter of the shish entities is generally smaller and their overall number-density per unit area is lower than in the fibers of class iii) because of the weaker elongational force (see Fig. 3(b‴) and (c‴)). This causes the lamellar overgrowth to form larger crystals than those in class iii), with an even larger averaged deviation angle θ of the stacking lamellae.

The fibers of class i) undergo almost no elongational influence on the molecular orientation through the whole spinning process and therefore any further lamellar crystal growth occurs mainly from the linking points keeping the initial random orientation (see Fig. 3(a‴)). In that case, crystallization may proceed by forming 3D-spherulitic structures rather than unoriented lamellae or crystallites.

3.2. Orientation analysis of beaded fibers

It has been suggested that the driving force of beaded fiber formation is based on two different types of axisymmetric instabilities by surface tension (classical Rayleigh mode) and electrical force (conducting mode) [6,7,38–41]. The formation of beaded fibers appears to be a common phenomenon in electrospinning of every kind of material. Usually, the formation of beaded fibers is not desired, however, some approaches for a beneficial application of a beaded morphology have been reported [42,43]. Thus, it is important to study the molecular and/or crystalline orientation in

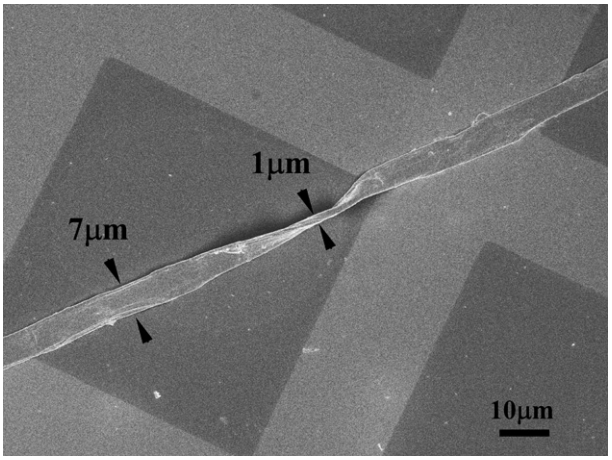

Fig. 9. SEM image showing a typical ribbon-like fiber. The spinning condition was 25 kV with a spinning distance of 300 mm.

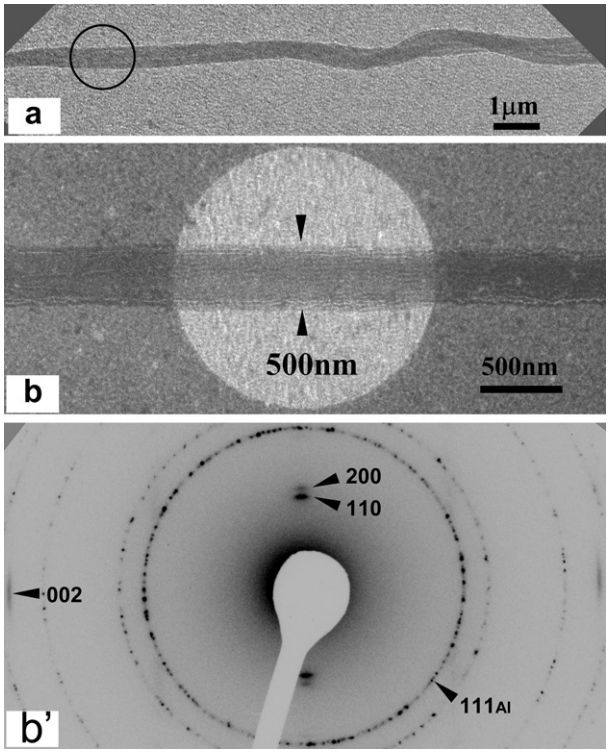

Fig. 10. SAED analysis of a thin ribbon-like fiber. The spinning conditions was 25 kV with a spinning distance of 300 mm. The grainy ring reflections in the SAED pattern are from the vapor-deposited aluminum (Al).

beaded fibers, especially the differences of structures between beaded and straight parts.

Fig. 8 shows an orientational analysis of a single beaded fiber composed of the straight part of about 700 nm diameter and the bead parts of about 8 μm diameter. The SAED pattern obtained from the straight part (Fig. 8(b)) shows an oriented crystalline pattern, while an unoriented sharp ring pattern is observed in the end of the bead part (Fig. 8(d)). In preliminary experiments with much thinner beaded fibers, whose bead parts were thin enough for analysis by TED, the crystalline structure in the center part of beads was also confirmed to be unoriented. On the other hand, the straight part (Fig. 8(c)) near the bead part shows an intermediate orientation degree between Fig. 8(b′) and (d′). This indicates that the molecular orientation changes gradually from the bead parts to the straight parts, i.e. the structural changes occur within a transition zone. These results indicate also that the XRD result by Rein et al. [17] included different orientational levels of the straight and the bead parts in the single beaded fibers.

3.3. Orientation analysis of ribbon-like fibers

During spinning from high-viscosity solution, frequently ribbon-like fibers are formed [44]. A typical SEM image of a ribbon 7 μm in width and 1 μm in thickness is shown in Fig. 9. According to Koombhongse et al. [45] those structures are preferably formed in cases where the skin part solidifies faster than the core part and when such a cylindrical skin-core structure is compressed into elliptical shape in cross-section by atmospheric pressure. The fine structure of those ribbon-like fibers has not been investigated so much [46,47].

A bright-field TEM image of a single ribbon-like fiber (width 480 nm; thickness 130 nm) and its SAED pattern are shown in Fig. 10. The rather sharp 110 and 200 equatorial reflections (with respect to the fiber axis) and the meridional 002 reflection indicate a high degree of molecular orientation. The somewhat changed intensity balance between the 110 and 200 reflections, as compared to the typical intensity balance in so-called fiber orientation as shown in e.g. Figs. 3(d′) and 6(g), and the lack of any another reflections, implies that the ribbon-like fibers do not have fiber texture but possess a tendency of uniplanar uniaxial orientation: probably that the long axis of such a ribbon is parallel to the *c*-axis and also the top and bottom surfaces are parallel to the (100) plane.

4. Conclusion

PE nanofibers with diameters as small as 150 nm, which reached the smallest diameter so far for PE, were successfully produced by high-temperature solution electrospinning. Individual orientation analysis by SAED for the various types of single nanofibers, which were produced in one and the same spinning process, revealed the formation of different types of fiber structure depending mainly on the fiber diameter, and also on the morphology.

A highly reproducible relationship has been found between the degree of molecular orientation and the fiber diameter, whereby the smaller fibers showed the more developed fiber structure. The basic structure of the cylindrical fibers is a shish-kebab structure and the differences in orientation can mainly be attributed to the differences of structurally averaged deviation angle of the *c*-axis in the kebab crystals from the direction of the fiber axis caused by curvature of lamellae. In contrast to the cylindrical fibers, beaded fibers were confirmed to have a different structure between the straight and bead parts in a single fiber, and the molecular orientation changes gradually from the bead part with unoriented structure to the straight part with an oriented one. We carried out the orientation analysis also for the single ribbon-like fibers and showed their highly ordered orientation.

Acknowledgements

We thank Prof. J.H.Wendorff (Marburg, Germany) for provision of research facilities. We also thank Prof. G. Sawers (Halle, Germany) for carefully reading the manuscript. T.Y. is grateful to Alexander von Humboldt Foundation (Germany) for a fellowship.

References

[1] Li D, Xia Y. Adv Mater 2004;16:1151–70.
[2] Ramakrishna S, Fujihara K, Teo WE, Lim TC, Ma Z. In: An introduction to electrospinning and nanofibers. Singapore: World Scientific Pub Co Pte Ltd; 2005. p. 275–340 [Chapter 7].
[3] Greiner A, Wendorff JH. Angew Chem 2007;46:5670–703.
[4] Reneker DH, Yarin AL, Fong H, Koombhongse S. J Appl Phys 2000;87:4531–47.
[5] Yarin AL, Koombhongse S, Reneker DH. J Appl Phys 2001;89:3018–26.
[6] Hohman MM, Shin M, Rutledge G, Brenner MP. Phys Fluids 2001;13:2201–20.
[7] Hohman MM, Shin M, Rutledge G, Brenner MP. Phys Fluids 2001;13:2221–36.
[8] Ramakrishna S, Fujihara K, Teo WE, Lim TC, Ma Z. In: An introduction to electrospinning and nanofibers. Singapore: World Scientific Pub Co Pte Ltd; 2005. p. 155–91 [Chapter 4].
[9] Reneker DH, Yarin AL. Polymer 2008;49:2387–425.
[10] Lim CT, Tan EPS, Ng SY. Appl Phys Lett 2008;92:141908–11.
[11] Bellan LM, Craighead HG. Polymer 2008;49:3125–9.
[12] Dersch R, Liu T, Schaper AK, Greiner A, Wendorff JH. J Polym Sci Part A 2003;41:545–53.
[13] Huang C, Chen S, Lai C, Reneker DH, Qiu H, Ye Y, et al. Nanotechnology 2006;17:1558–63.
[14] Keum JK, Zuo F, Hsiao BS. Macromolecules 2008;41:4766–76.
[15] Larrondo L, Manley RStJ. J Polym Sci Polym Phys Ed 1981;19:909–20.
[16] Givens SR, Gardner KH, Rabolt JF, Chase DB. Macromolecules 2007;40:608–10.
[17] Rein DM, Shavit-Hadar L, Khalfin RL, Cohen Y, Shuster K, Zussman E. J Polym Sci Part B Polym Phys 2007;45:766–73.
[18] Rein DM, Cohen Y, Ronen A, Shuster K, Zussman E. Polym Eng Sci 2009;49:774–82.
[19] Kakade MV, Givens S, Gardner K, Lee KH, Chase DB, Rabolt JF. J Am Chem Soc 2007;129:2777–82.
[20] Kongkhlang T, Tashiro K, Kotaki M, Chirachanchai S. J Am Chem Soc 2008;130:15460–6.
[21] Amano T. Flow-induced crystallization in polymer systems. In: Miller RL, editor. Midland macromolecular monographs, vol 6. Gordon and Breach; 1979. p. 119–24.
[22] Pennings AJ, Kiel AM. Kolloid-Z Z Polym 1965;205:160–2.
[23] Pennings AJ. J Polym Sci Polym Symp 1977;59:55–86.
[24] Wang B, Li B, Xiong J, Li CY. Macromolecules 2008;41:9516–21.
[25] Zussman E, Rittel D, Yarin AL. Appl Phys Lett 2003;82:3958–60.
[26] Nagou S, Azuma K. J Macromol Sci Phys 1979;B16:435–48.
[27] Popli R, Roylance D. Polym Eng Sci 1985;25:828–33.
[28] Peterlin A. Colloid Polym Sci 1975;253:809–23.
[29] Adams WW, Yang D, Thomas EL. J Mater Sci 1986;21:2239–53.
[30] Brady JM, Thomas EL. J Mater Sci 1989;24:3311–8.
[31] Plummer CJG, Cudre-Mauroux N, Kausch HH. Polym Eng Sci 1994;34:318–29.
[32] Zuo F, Keum JK, Chen X, Hsiao BS, Chen H, Lai SY, et al. Polymer 2007;48:6867–80.
[33] Barham PJ, Keller A. J Mater Sci 1985;20:2281–302.
[34] Smith P, Lemstra PJ. J Mater Sci 1980;15:505.
[35] Yoshioka T, Tsuji M, Kawahara Y, Kohjiya S, Manabe N, Yokota Y. Polymer 2005;46:4987–90.
[36] Li L, Yang Y, Yang G, Chen X, Hsiao BS, Chu B, et al. Nano Lett 2006;6:1007–12.
[37] Li L, Li B, Hood MA, Li CY. Polymer 2009;50:953–65.
[38] Fong H, Chun I, Reneker DH. Polymer 1999;40:4585–92.
[39] Zuo W, Zhu M, Yang W, Yu H, Chen Y, Zhang Y. Polym Eng Sci 2005;45:704–9.
[40] Eggers J, Villermaux E. Rep Prog Phys 2008;71:036601–79.
[41] Carroll CP, Joo YL. Phys Fluids 2009;21:103101.
[42] Tomczak N, van Hulst NF, Vancso GJ. Macromolecules 2005;38:7863–6.
[43] Yoon YI, Moon HS, Lyoo WS, Lee TS, Park WH. J Colloid Interface Sci 2008;320:91–5.
[44] Koski A, Yim K, Shivkumar S. Mater Lett; 2004:493–7.
[45] Koombhongse S, Liu W, Reneker DH. J Polym Sci Part B Polym Phys 2001;39:2598–606.
[46] Guenthner AJ, Khombhongse S, Liu W, Dayal P, Reneker DH, Kyu T. Macromol Theory Simul 2006;15:87–93.
[47] Tosaka M, Yamaguchi K, Tsuji M. Polymer 2010;51:547–53.